Finite volume fraction effect on self-induced velocity in two-way coupled Euler-Lagrange simulations

Jungyun Kim and S. Balachandar*
University of Florida, Gainesville, Florida 32611, USA

(Received 20 January 2024; accepted 29 February 2024; published 27 March 2024)

In a two-way coupled Euler-Lagrange (EL) simulation, a particle of size comparable to the local grid spacing results in self-induced perturbation, which must be subtracted to obtain the undisturbed velocity of the particle. Several approaches have been advanced to estimate the self-induced velocity in the limit of an isolated particle. The present work addresses the effect of nonzero volume fraction in predicting the self-induced velocity of particles in an EL simulation. In addition to performing EL simulations of flow over a random distribution of stationary particles, we also perform several hundred companion simulations covering a range of Reynolds number and volume fraction. In each companion simulation we have removed one particle from the random distribution whose undisturbed flow and self-induced velocities are thereby precisely computed. By analyzing the self-induced velocity obtained from these simulations, a number of key conclusions are drawn. The most significant of them is the finding that the self-induced correction procedure of an isolated particle can be applied even at a finite volume fraction, with a simple volume fraction dependent modification, in order to accurately capture the average behavior.

DOI: 10.1103/PhysRevFluids.9.034306

I. INTRODUCTION

The importance of correcting for the self-induced perturbation in an Euler-Lagrange (EL) simulation when the particle is of comparable size to the local grid has now been widely recognized [1–24]. In essence, for particles of size comparable to the local grid, the feedback force of the particle strongly influences the local momentum balance within the grid cell, and as a result, the local fluid velocity within the cell is substantially different from that in the absence of the feedback force (i.e., in the absence of the particle). However, the standard point-particle drag models have been developed to predict the force on a particle given either the ambient fluid velocity far away from the particle or the undisturbed fluid velocity that would exist in the absence of the particle. Therefore, in the case of particles of a size comparable to the grid, the standard drag models, when applied with the local fluid velocity within the grid cell computed in the EL methodology, will not accurately predict the force on the particle.

In fact, in general, since the feedback force on the fluid opposes the relative velocity of the fluid as seen by the particle, the local fluid velocity computed in an EL simulation will be smaller than what it would be in the absence of the particle, thus resulting in an underestimation of the particle force. As illustrated by Horwitz and Mani [13], as the particle approaches the grid size, the underestimation of error can be in excess of 50%. A simple approach to avoiding this error is to calculate the drag force on the particle not using the local fluid velocity calculated in the EL simulation, but using a corrected local fluid velocity, which better approximates the undisturbed fluid velocity. This corrected undisturbed fluid velocity is obtained by removing from the local EL

*Corresponding author: bala1s@ufl.edu

fluid velocity the self-induced velocity due to the feedback force of the particle, i.e., by removing the feedback presence of the particle, the undisturbed flow at the particle can be better represented.

The above-referenced papers offer a variety of approaches to estimating the self-induced velocity of a particle. These approaches include an analytical solution derived by solving the unsteady Stokes equation [4,10], Oseen's solution of a Gaussian force applied to a uniform flow or regularized Oseen solution [1,2,7,18], a discrete Green's function solution [12], a solution by interpolation kernels [16], and solving the model advection-diffusion-reaction equation [25]. These analytical approaches are generally independent of the details of numerical discretization, with the assumption that the Gaussian or other regularization functions are adequately numerically resolved. There have also been solutions to estimating the self-induced velocity of a particle that are built upon numerical implementations [13–15,21,22].

All the above efforts of self-induced velocity estimation have been for an isolated particle in a uniform ambient flow. In an unsteady flow, the steady approach must be applied in a quasisteady manner, based on the instantaneous flow at the particle location. Quasisteady approaches are adequate in slowly varying flows. The effect of unsteadiness has been explicitly accounted for in the estimation of self-induced velocity either with analytical solutions of the unsteady Stokes equation [3,4,7,10] or with a convolution integral whose kernel has been empirically obtained from finite Reynolds number simulations [1,2,18]. The numerically based correction procedures [13–15,21,22] enjoy the advantage that they can be readily implemented in unsteady flows. Other effects, such as the influence of a nearby wall, have also been considered [1,22].

The natural next step of broadening the applicability of the above-discussed self-induced velocity estimation procedures is to consider problems involving random distributions of particles. A number of questions arise in the presence of other nearby neighbors. Foremost among them is, how important is the self-induced correction at a finite volume fraction, where the computed EL flow at a particle is influenced not only by the self-induced perturbation of that particle, but also by the perturbation effect of all its neighbors? If important, can the current methods be generalized to conditions of finite particle volume fraction? Can the estimation procedure developed for an isolated particle be applied even in the case of a finite volume fraction?

The focus of the present paper is to address the above questions and thereby extend the existing isolated-particle-based understanding of self-induced velocity correction to finite volume fraction conditions. This will be accomplished by isolating the self-induced velocity perturbation of individual particles that are members of a random distribution subjected to a uniform flow. The self-induced velocity of an isolated particle has been readily calculated by subtracting the local fluid velocity at the particle computed in an EL simulation from the ambient uniform flow. This approach is not possible with a distribution of particles since the difference between the local fluid velocity at the particle and the ambient uniform flow derives contributions not only from the self-induced perturbation of the particle, but also from the perturbations of all the neighbors.

In fact, plots of velocity perturbation calculated with the feedback force of an isolated particle represented as a Gaussian force were presented in [2] for a range of Reynolds numbers. These plots clearly show that the perturbation flow due to a Gaussian forcing extends several particle diameters downstream, with the length of the wake increasing with the Reynolds number. Furthermore, the peak velocity perturbation is not at the center of the perturbing particle, but at some distance downstream. Thus, it can be expected that in a distribution of particles, the neighbor influence can be substantial and often far in excess of self-induced perturbation.

Here we perform several hundred simulations with and without the presence of individual particles in order to carefully isolate the self-induced perturbation velocity. The results have allowed us to answer the following questions: (i) How important is self-induced perturbation compared to the perturbation effect of neighbors at varying values of Reynolds number and volume fraction? (ii) Does self-induced velocity averaged over many particles depend on volume fraction, in addition to being a function of Reynolds number and feedback force magnitude? (ii) How does the self-induced velocity of individual particles deviate from the average behavior (similar to drag of an individual particle in a random distribution being different from the average)?

An important limitation of the present investigation must be emphasized. While we will gain a better understanding of the self-induced flow at a finite volume fraction, this will not necessarily lead to a better deterministic force model. Since the perturbation influence of the neighbors as computed in an EL simulation will not capture the actual perturbation as in a PR simulation, even without the self-perturbation effect, the undisturbed flow of a particle in an EL simulation will not be the same as the true value of a PR simulation. This difference must first be well understood in order to develop better EL predictive force models. In contrast, in the case of an isolated particle, an improved understanding of self-induced velocity immediately led to better force prediction. Nevertheless, here we will investigate the effect of particle volume fraction on self-induced perturbation, following the methodology of our previous work [1,2]. However, the conclusion to be drawn applies equally to all other correction methods as well.

The rest of the paper is arranged as follows. First we will present the statement of the problem and the EL numerical methodology to be pursued in Sec. II. The results are then presented and analyzed in Sec. III. Finally, in Sec. IV we draw the conclusions.

II. STATEMENT OF THE PROBLEM

Consider a triply periodic cubic domain of size L^3. Inside is a random distribution of N stationary particles of diameter d_p, such that we achieve the desired average volume fraction of $\langle\phi_p\rangle = N\pi d_p^3/(6L^3)$. The particles are distributed with uniform probability using the random insertion algorithm. In the EL simulation, the interfaces between the particles and the surrounding fluid are not resolved, and only the filtered governing equations of the flow are solved. The filtered particle volume fraction field is defined as

$$\phi_p(\mathbf{x}) = \int I_p(\mathbf{x}')\, G(\mathbf{x}-\mathbf{x}')\, d\mathbf{x}'. \tag{1}$$

The corresponding complementary fluid volume fraction is given by $\phi_f(\mathbf{x}) = 1 - \phi_p(\mathbf{x})$. In the present problem, they are time-independent since the particles are stationary. In the above, I_p is the indicator function that is unity inside the region occupied by the particles (i.e., $I_p = 1$ for $|\mathbf{x} - \mathbf{X}_l| < d_p/2$, $l = 1, \ldots, N$, where $\mathbf{X}_l$ is the position of the lth particle) and zero everywhere outside. Also, the integral is over the entire triply periodic box. We take the filter function used in regularization to be an isotropic Gaussian [2,26]:

$$G(\boldsymbol{\xi}) = \frac{1}{(2\pi)^{3/2}\sigma^3} \exp\left(-\frac{|\boldsymbol{\xi}|^2}{2\sigma^2}\right), \tag{2}$$

where σ is the parameter that controls the width of the Gaussian. With this definition, Eq. (1) can be integrated and the volume fraction field can be expressed as

$$\phi_p(\mathbf{x}) = \sum_{l=1}^{N} \phi_1(\mathbf{x}-\mathbf{X}_l) = \sum_{l=1}^{N} \frac{\mathrm{erf}(A_l) - \mathrm{erf}(B_l)}{2} + \frac{\exp\left(-A_l^2\right) - \exp\left(-B_l^2\right)}{\sqrt{\pi}(A_l + B_l)}, \tag{3}$$

where $A_l = (2|\mathbf{x} - \mathbf{X}_l| + d_p)/(2\sqrt{2}\sigma)$ and $B = (2|\mathbf{x} - \mathbf{X}_l| - d_p)/(2\sqrt{2}\sigma)$. Since the particle volume fraction field is a superposition of that due to each of the particles, the corresponding fluid volume fraction ϕ_f has local minima at the center of the particles and increases away from the particles. It should be noted that for particles that are close to the sides of the periodic box, the Gaussian is extended on the other side to properly satisfy periodicity. With the above definition, the condition $\int \phi_p(\mathbf{x})\, d\mathbf{x} = \langle\phi_p\rangle$ is strictly satisfied. In this study, we have chosen $\sigma/d_p = 2$, and the effect of this parameter will be discussed later.

A mean streamwise pressure gradient along the positive x-direction drives a mean flow U along this direction. In the EL simulations and the subsequent analysis, σ is chosen as the length scale,

TABLE I. List of simulation cases considered.

Volume fraction ($\langle\phi_p\rangle$)	The number of particles (N)	Box size (L)	Gaussian parameter (σ)	Re_σ	Particle diameter (d_p)	Feedback force (F)
0.0015	1000	35.2052	1	1, 10, 100	0.5	1
0.01	6666	35.2052	1	1, 10, 100	0.5	1
0.033	22000	35.2052	1	1, 10, 100	0.5	1
0.1	66667	35.2052	1	1, 10, 100	0.5	1

and the mean fluid velocity within the box is chosen as the velocity scale. This yields $\mathrm{Re}_\sigma = \sigma U/\nu$. The corresponding time, pressure, and force scales are σ/U, ρU^2, and $\rho U^2\sigma^2$. We consider each particle to be applying a unit nondimensional feedback force along the negative x-direction on the surrounding fluid. The forces are applied using the Gaussian function, and the resulting three-dimensional feedback force field can be expressed as

$$\mathbf{F}_{p\to f}(\mathbf{x}) = \sum_{l=1}^{N} \mathbf{F}_l = -\sum_{l=1}^{N} \mathbf{e}_x G(\mathbf{x}-\mathbf{X}_l), \tag{4}$$

where $\mathbf{e}_x$ is the unit vector along the x-direction. This is just a simple model to help us understand the nature of self-induced flow in the context of finite volume fraction. It does not account for the shielding/drafting effect.

While the geometry is triply periodic, the flow is solved with periodic boundary conditions along the lateral y and z directions. A constant unit inflow is applied along the x-direction and the flow is allowed to freely exit without reflections along the outflow. An alternate approach is to apply periodicity in the streamwise direction as well and choose the velocity scale to be such that streamwise pressure gradient is unity. The relative merits of the two approaches are known. By imposing the mean flow velocity to be unity, we strictly control the mean flow Reynolds number. On the other hand, the particles near the inlet and outlet boundaries are excluded from the statistics. The interior region that was chosen for statistical averaging was determined to ensure that the results are converged and are in agreement with the results of periodic boundary conditions (periodic simulation required iteration to match the mean flow Reynolds number).

The governing filtered fluid equations solved in the Euler-Lagrange numerical simulations are

$$\begin{aligned} \nabla\cdot(\phi_f\mathbf{u}) &= \mathbf{0}, \\ \frac{\partial\mathbf{u}}{\partial t} + \mathbf{u}\cdot\nabla\mathbf{u} &= -\nabla p + \frac{1}{\mathrm{Re}_\sigma}\nabla^2\mathbf{u} + \frac{\mathbf{F}_{p\to f}}{\phi_f}, \end{aligned} \tag{5}$$

where the variables are nondimensional. In the above filtered EL equations, $\mathbf{u}$ is the phase-averaged fluid velocity that has been averaged over the fluid phase, and we have ignored the Reynolds stress and the residual viscous terms.

The three important parameters of the numerical simulation are the Reynolds number Re_σ, the average volume fraction $\langle\phi_p\rangle$, and the nondimensional feedback force applied by the particles. We consider three different Reynolds numbers $\mathrm{Re}_\sigma = 1$, 10, and 100, and four different volume fractions $\langle\phi_p\rangle = 0.0015$, 0.01, 0.033, and 0.1. The nondimensional feedback force is chosen to be unity along the negative x-direction. The periodic box size is chosen to be $L/\sigma = 35.2052$, so that the number of particles with the periodic box is 1000, 6666, 22 000, and 66 667, respectively. This information along with other details of the different simulations are presented in Table I. All simulations are computed using the spectral element code Nek5000 [27,28] with a discretization of $12\times12\times12$ spectral elements and $6\times6\times6$ Legendre-Gauss-Lobatto grid points within each element. Due to the smooth nature of the Gaussian forcing, the flow fields are smooth as well and therefore a

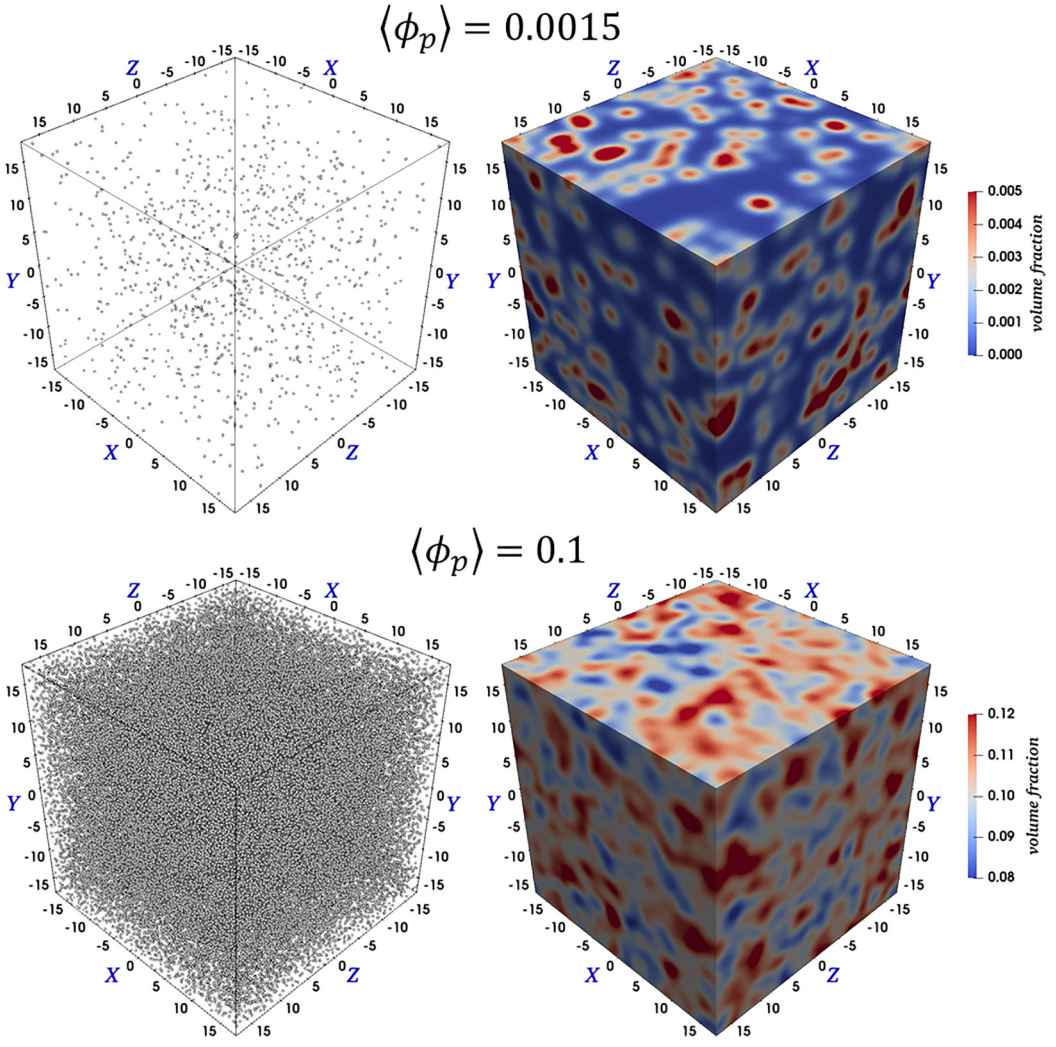

FIG. 1. Particle distribution within the triply periodic box and contours of particle volume fraction field at $\langle \phi \rangle = 0.0015$ (top row) and $\langle \phi \rangle = 0.1$ (bottom row). It should be noted that for visualization purposes, the particles are not drawn to scale.

modest grid is sufficient to adequately resolve the flow. Grid independence has been established in all the cases to be presented.

A sample distribution of particles and the corresponding volume fraction on three different planes within the domain for the low and high volume fractions of $\langle \phi_p \rangle = 0.0015$ and 0.1 are presented in Fig. 1. The rms volume fraction variations within the entire volume of the domain for the four different volume fractions considered in this study are 0.001 343, 0.003 35, 0.005 874, and 0.0077, respectively. This variation is due to the random distribution of particles. Furthermore, the observed variation is dictated by the half-width of the Gaussian function, which is chosen to be $2.35d_p$. A simple estimate of mean particle separation can be obtained as $(\pi/6\phi_p)^{1/3}d_p$, which yields mean separation distances of 7.04, 3.74, 2.51, and 1.74 at the four different volume fractions. A comparison of these distances with the Gaussian width explains the higher volume fraction variation relative to the mean volume fraction at small values of $\langle \phi_p \rangle$. Nevertheless, as

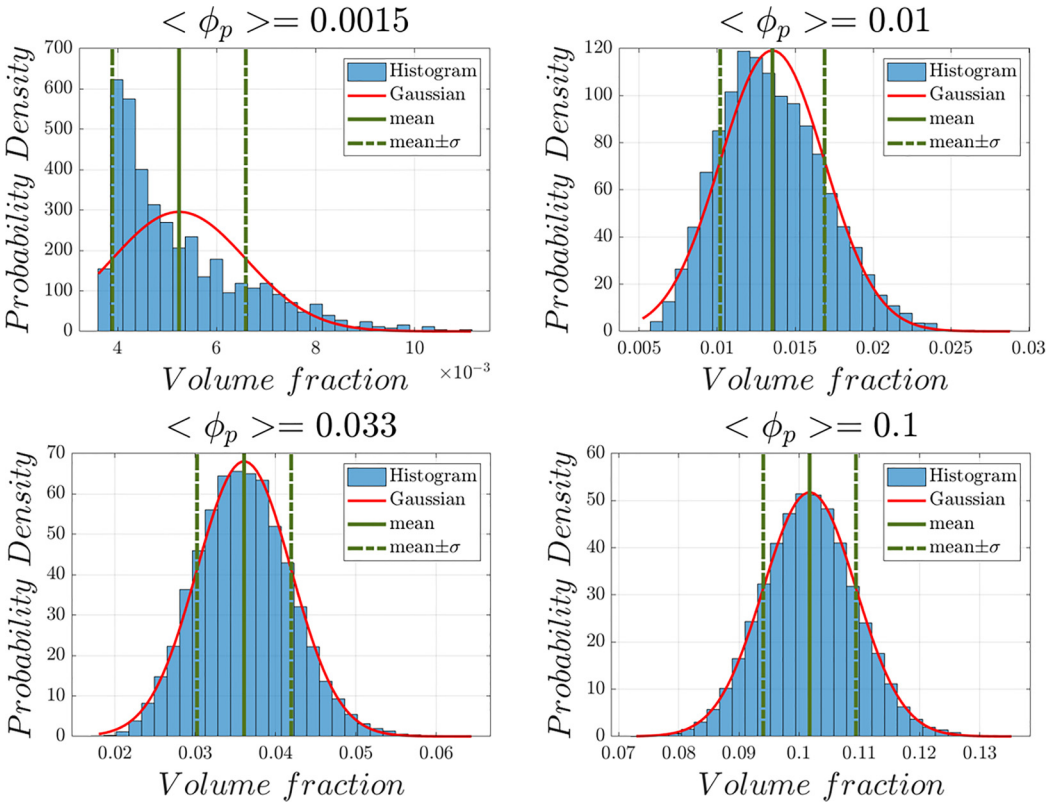

FIG. 2. Histogram of volume fraction field evaluated at the particle centers. The results are shown for four different values of average volume fraction. Gaussian fits are plotted in red. The mean and one standard deviation on either side are shown.

a result of this variation, some particles happen to be in regions of higher local volume fraction surrounded by many close neighbors than others whose local volume fraction is lower than the average. In all the cases, the particle volume fraction averaged over the entire box is equal to the average value.

The volume fraction at the lth particle is denoted as $\phi_{p,l} = \phi_p(\mathbf{X}_l)$. The mean Lagrangian particle volume fractions averaged over all the particle centers for the four average volume fractions are $\langle \phi_p \rangle_L = 0.005\,22$, $0.013\,53$, $0.036\,07$, and $0.101\,74$, respectively. These are higher than the corresponding domain averages. If we denote the self-induced volume fraction of an individual particle at its own center to be $\phi_1(\mathbf{x} = \mathbf{0})$ for $d_p/\sigma = 1/2$, we obtain $\phi_1(\mathbf{x} = \mathbf{0}) = 0.004\,08$. Thus, deviation from this value is the contribution to volume fraction from all other neighbors. This explains $\langle \phi_p \rangle_L$ being substantially larger than the Eulerian average $\langle \phi_p \rangle$ in the limit of $\langle \phi_p \rangle \to 0$. Another reason we expect $\langle \phi_p \rangle_L$ to be greater than $\langle \phi_p \rangle$ is because more particles are in regions of higher volume fraction, and as a result an average over particles will lead to a higher value [29]. The difference between the Lagrangian and domain-averaged volume fraction is generally small at larger volume fraction. Nevertheless, it must be noted that the average volume fraction seen by the particles will be higher than the domain average.

Figure 2 shows the normalized histogram of particle volume fraction $\phi_{p,l}$ for all four volume fractions. The mean is marked along with the range denoting one standard deviation. At $\langle \phi_p \rangle = 0.0015$, the Lagrangian volume fraction distribution is positively skewed, and due to the limited sample size, the distribution is somewhat noisy. With increasing mean volume fraction, the distributions become

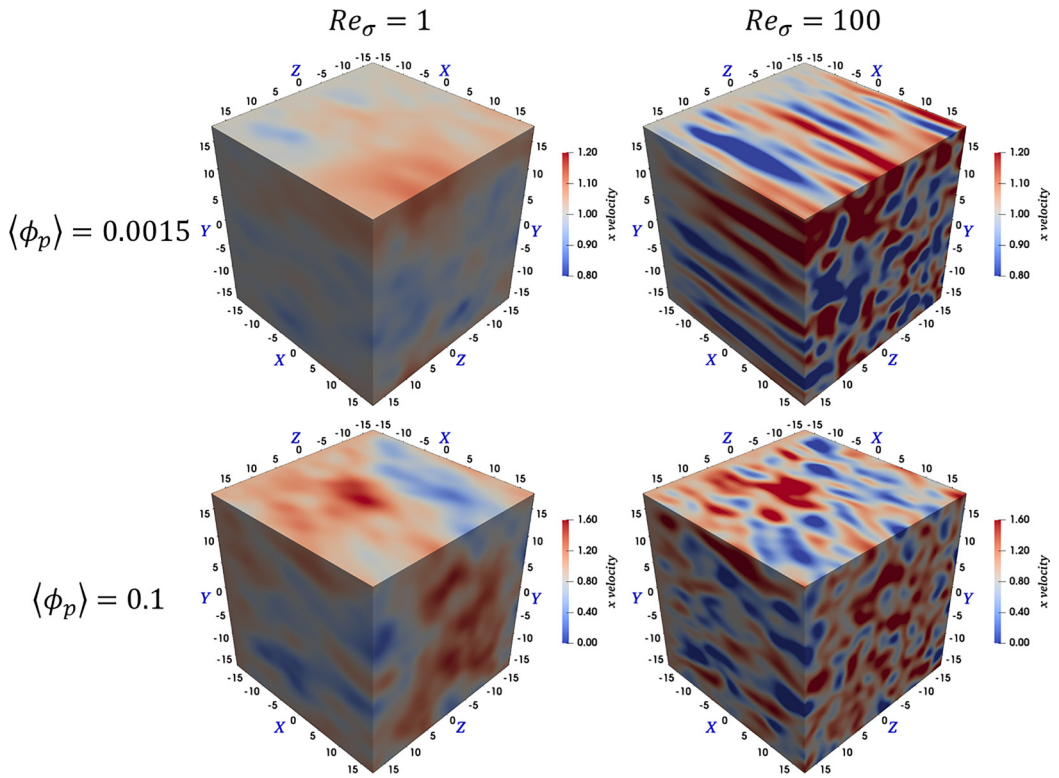

FIG. 3. Contours of fluid velocity computed in the EL simulation with feedback force applied at all the particles. The results are shown for two different mean Reynolds numbers and volume fraction.

smooth and are well approximated by a Gaussian. The standard deviations of Lagrangian volume fraction for the four different cases are 0.001 34, 0.003 35, 0.005 86, and 0.007 71, respectively.

The simulated streamwise velocity contours on three different planes within the domain for the low and high volume fractions of $\langle \phi_p \rangle = 0.0015$ and 0.1 for $\mathrm{Re}_\phi = 1$ and 100 are presented in Fig. 3. Several observations can be made. The velocity perturbation due to the feedback from the particles increases both with volume fraction and Reynolds number. Although the particles are many in number with increasing volume fraction, the level of spatial complexity of the flow does not scale with the number of particles, since the force feedback has been smoothed with the Gaussian, whose size remains the same in all cases. For the $\mathrm{Re}_\sigma = 100$ cases there is long streamwise coherence in the perturbation flow, which is due to the very long wake structure of individual particles at higher Reynolds number, as observed in the isolated particle simulations of [2]. This streamwise coherence somewhat decreases at the higher volume fraction due to the higher interference of the downstream particles.

Note that the EL simulations compute the fluid velocity over the entire domain, even in the regions occupied by the particles. In fact, the drag force on the particles is typically calculated based on the fluid velocity evaluated (or interpolated) at the particle center. From Fig. 3 it can be seen that fluid velocity at the particle location deviates from the mean nondimensional value of unity. This deviation increases with $\langle \phi_p \rangle$ and Re_σ. Let the fluid velocity at the location of the lth particle computed in the EL simulation be $\mathbf{u}_{@l} = \mathbf{u}(\mathbf{X}_l)$. Figure 4 shows the normalized histogram of streamwise velocity perturbation $(1 - \mathbf{u}_{@l} \cdot \mathbf{e}_x)$ for all four volume fractions and three Re_σ. The mean is marked along with the range denoting the standard deviation. The histograms are smoother for the higher volume fraction cases due to the availability of many more particle samples. All the

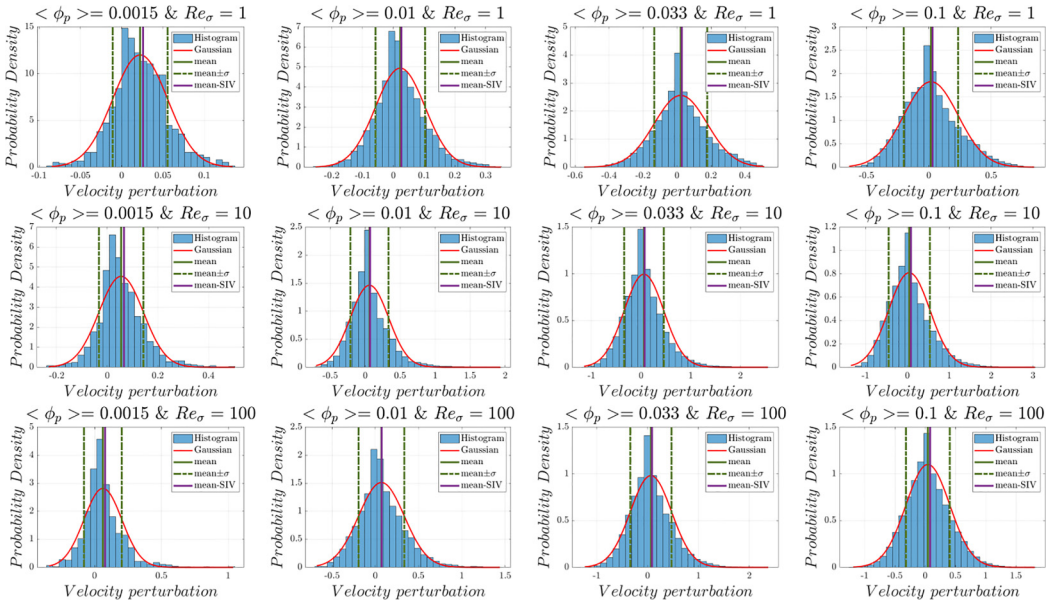

FIG. 4. Histogram of deviation from unity in the streamwise component of fluid velocity measured at the particle centers obtained for all 12 cases considered. The Gaussian fits are shown in red. Again the mean and one standard deviation are shown, along with the mean computed without the self-induced velocity perturbation, which is denoted as "mean-SIV."

distributions are positively skewed, with the peaks slightly shifted to the left of the mean value. The normalized histograms are also faster decaying than the Gaussian distribution. It should be noted that this velocity distribution is unique to the idealized case of unit forcing being investigated in the present study. In a typical EL simulation, the feedback force of a particle is a variable and depends on the particle Reynolds number and local volume fraction.

An interesting aspect of EL simulations at finite volume fraction is the nonzero value of the resulting velocity field. From the mass balance equation given in (5), we obtain $\nabla \cdot \mathbf{u} = (\mathbf{u} \cdot \nabla \phi_p)/(1 - \phi_p)$. Contours of this quantity are plotted in Fig. 5 for $\mathrm{Re}_\sigma = 1$ for the four different volume fractions considered. From the figure it is clear that fluid velocity divergence is quite small at low volume fractions. At an average volume fraction of 10%, divergence is still small only at 0.01. Thus, in all the results to be discussed in this work, the importance of velocity divergence due to random particle distribution is not large.

III. RESULTS—SELF-INDUCED VELOCITY

In the absence of particles (i.e., $\phi_f = 1$) and the feedback force $\mathbf{F}_{p\to f}$, the flow over the entire domain would have been the unit vector $\mathbf{e}_x$. The difference $\mathbf{e}_x - \mathbf{u}_{@l}$ is the effect of all the particles. Part of it is due to the self-induced perturbation arising from the feedback force of the lth particle. There is also the effect of perturbation flow due to the neighbor's feedback forces.

Separation of the self-induced perturbation of a particle from the perturbative effect of all the neighbors is the focus of this study. In the present work, we achieve this separation by performing many companion $(N-1)$-particle simulations, in each of which the steady flow is computed with all the particles except one. For each $(\mathrm{Re}_\sigma, \langle\phi_p\rangle)$ case listed in Table I, we perform $M = 30$ simulations, and in each of these simulations one particle at random is removed from the simulation (i.e., the volume effect and the Gaussian feedback force of this particle are not applied). The resulting flow will be denoted as $\mathbf{u}^{\mathrm{un}}(\mathbf{x})$ and the fluid velocity at the removed lth particle will be denoted as

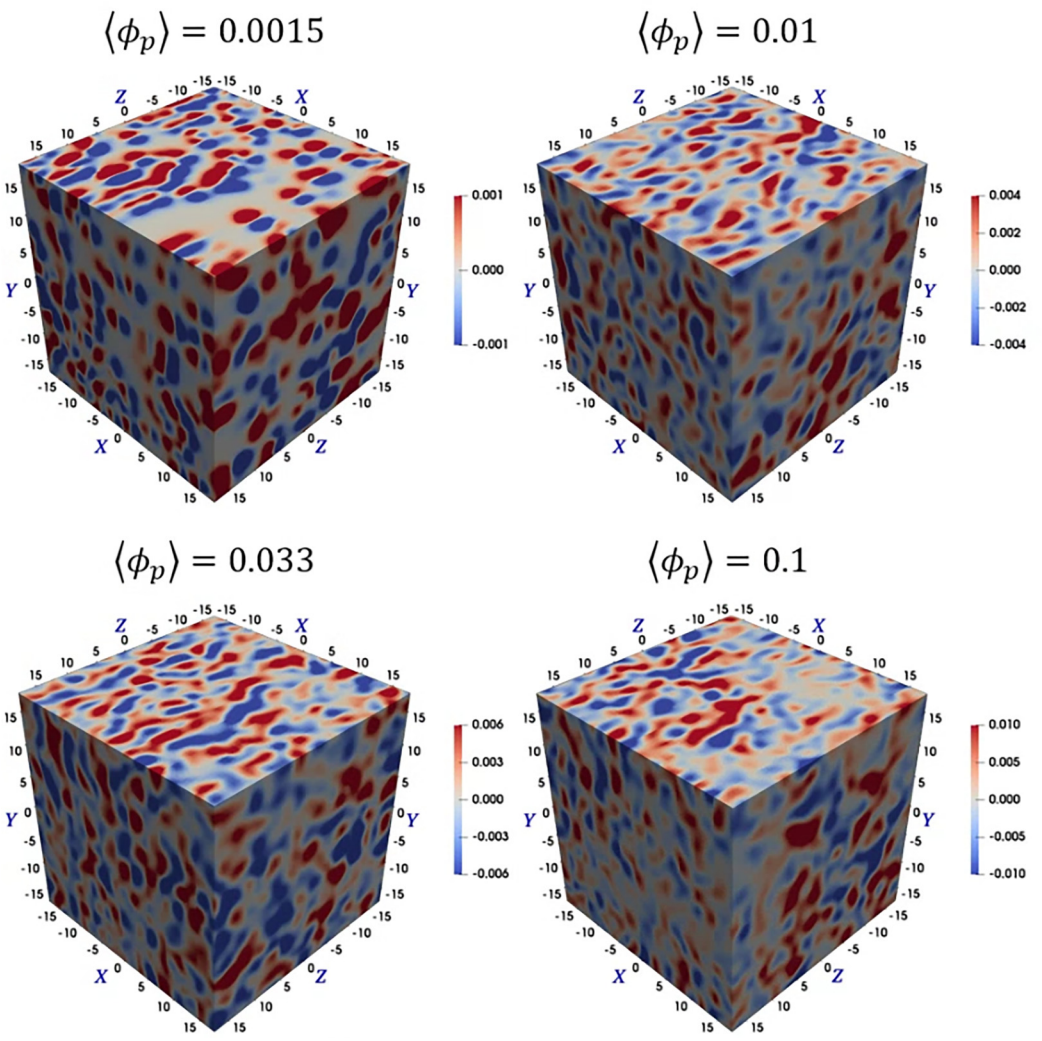

FIG. 5. Contours of fluid velocity divergence for the four different volume fraction distributions at $\mathrm{Re}_\sigma = 1$. The results are qualitatively similar at other Reynolds numbers.

$\mathbf{u}^{\mathrm{un}}_{@l} = \mathbf{u}^{\mathrm{un}}(\mathbf{x} = \mathbf{X}_l)$. With this, the self-induced velocity of the lth particle can be computed as

$$\mathbf{u}^{\mathrm{si}}_{@l} = \mathbf{u}_{@l} - \mathbf{u}^{\mathrm{un}}_{@l}. \tag{6}$$

The interpretation is as follows. In the absence of all two-way coupling effects, the nondimensional flow would be the constant vector $\mathbf{e}_x$. In the presence of all the neighbors, but without its own presence, the velocity at $\mathbf{X}_l$ is $\mathbf{u}^{un}_{@l}$. This is the undisturbed velocity of the lth particle as calculated in the EL simulation, which in general will not be the same as what one would obtain in a PR simulation. The velocity $\mathbf{u}_{@l}$ includes the added self-induced effect of the lth particle, which can be isolated with the equation given above. The biggest drawback of the above approach is that with each additional companion simulation, we obtain the self-induced velocity of only one particle. Thus, conclusions need to be drawn with only a small set of self-induced velocities (i.e., for small values of M). Here the volume fraction effects are investigated with 372 simulations (for $M = 30$). It should be noted that when the lth particle is removed, it is not only the fluid velocity at the

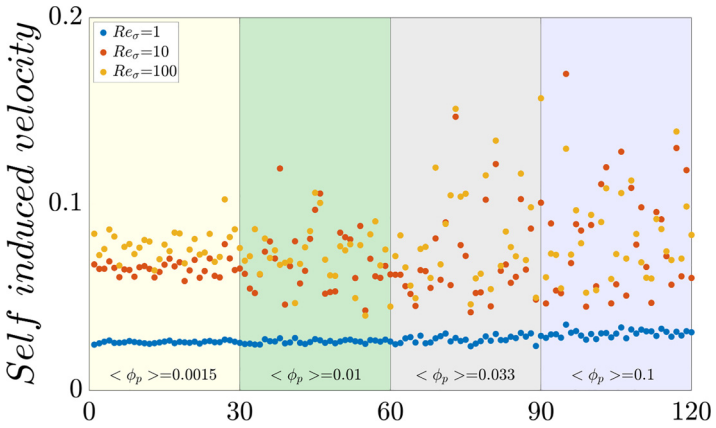

FIG. 6. Self-induced velocity from all 360 $(N-1)$-particle simulations.

removed particle that changes due to self-induced perturbation. The velocity at all other particles also changes slightly, due to the removal of the lth particle. However, this change is far smaller than the change in the velocity at the location of the removed particle.

Figure 6 plots the x-component of the self-induced velocity, where the first M points are $\langle\phi_p\rangle = 0.0015$, the next M are $\langle\phi_p\rangle = 0.01$, etc. The three Re_σ are plotted in different colors. The different shaded vertical bands separate the different $\langle\phi_p\rangle$ values. It is clear from the plots that the self-induced velocities of the M particles are not exactly the same. Substantial particle-to-particle variation in self-induced velocity is observed, the amplitude of which increases with increasing volume fraction. The increase in self-induced velocity with increasing Re_σ is expected based on observations made in earlier studies of isolated particles. Fortunately, the effect of mean particle volume fraction on average self-induced velocity is not strong, although a slight increase with increasing volume fraction can be observed. The mean values of the self-induced velocity (denoted as $u^{\mathrm{SI},S}_{@l}$) computed based on the $M = 30$ samples are presented in Table II for the different combinations of $\langle\phi_p\rangle$ and Re_σ. The corresponding standard deviation is presented in parentheses. These mean values are presented in Fig. 4 as "mean-SIV," while the "mean" in the figure corresponds to the average total velocity perturbation at the particles, including both the self-induced contribution as well as the perturbation from neighbors. It should be noted that the mean and standard deviation presented in Table II are based on the limited sample of only 30 particles. Assuming a Gaussian distribution for the self-induced perturbation velocity, from statistical theory, the sample mean can be expected to follow the t-distribution and the variance to follow the χ^2 distribution. The corresponding confidence intervals of both that mean and the standard deviation are also presented in Table II.

The standard deviation of self-induced velocity goes to zero with decreasing volume fraction. At the lowest Reynolds number considered, the standard deviation is less than about 7% of the mean at all volume fractions considered. At higher Re_σ, standard deviation increases to about 35% of the mean, at higher volume fractions. Nevertheless, the range of self-induced velocities measured at the 30 particles is much smaller than the range of velocity perturbations due to the neighbor influence seen in Fig. 6. In other words, for any particle within a random distribution, the perturbation effect of its neighbors will often be far larger than the self-induced perturbation of the particle on itself.

It may therefore be tempting to conclude that the self-induced velocity correction of a particle can be ignored with increasing volume fraction. While this may be true at the level of individual particles, the same does not hold in the statistical sense. When averaged over all the particles, the perturbation effect of the neighbors becomes zero, while the self-induced perturbation has a finite value, which in Table II can be as large as 8.5%. In other words, the influence of neighbors, though it can be large in magnitude, varies from positive to negative values for different particles, depending

TABLE II. The mean and standard deviation (shown in parentheses) of the self-induced velocity of the $M = 30$ samples. Also presented are the 95% confidence intervals.

	$u_{@l}^{\mathrm{si},S}$			$u_{@l}^{\mathrm{si},M}$		
$\langle\phi_p\rangle$	$\mathrm{Re}_\sigma = 1$	$\mathrm{Re}_\sigma = 10$	$\mathrm{Re}_\sigma = 100$	$\mathrm{Re}_\sigma = 1$	$\mathrm{Re}_\sigma = 10$	$\mathrm{Re}_\sigma = 100$
0.0015	0.0259	0.0657	0.0779	0.0285	0.0710	0.0826
	(0.00060)	(0.00405)	(0.00744)	(0.00046)	(0.00060)	(0.00014)
0.01	0.0263	0.0698	0.0721	0.0290	0.0702	0.0821
	(0.00098)	(0.01731)	(0.01459)	(0.00144)	(0.00409)	(0.00362)
0.033	0.0275	0.0706	0.0849	0.0297	0.0710	0.0837
	(0.00197)	(0.02388)	(0.02925)	(0.00319)	(0.00933)	(0.00358)
0.1	0.0306	0.0814	0.0817	0.0335	0.0742	0.0879
	(0.00188)	(0.03071)	(0.02146)	(0.00338)	(0.01123)	(0.00659)

95% confidence interval of $u_{@l}^{\mathrm{si},S}$

$\langle\phi_p\rangle$	$\mathrm{Re}_\sigma = 1$	$\mathrm{Re}_\sigma = 10$	$\mathrm{Re}_\sigma = 100$
0.0015	0.0257; 0.0262	0.0642; 0.0672	0.0751; 0.0807
	(0.00048; 0.00082)	(0.00328; 0.00554)	(0.00603; 0.01017)
0.01	0.0259; 0.0266	0.0632; 0.0764	0.0665; 0.0776
	(0.00079; 0.00134)	(0.01402; 0.02367)	(0.01182; 0.01995)
0.033	0.0268; 0.0283	0.0615; 0.0796	0.0738; 0.0960
	(0.00159; 0.00269)	(0.01935; 0.03265)	(0.02369; 0.03999)
0.1	0.0299; 0.0313	0.0698; 0.0931	0.0735; 0.0898
	(0.00152; 0.00257)	(0.02487; 0.04198)	(0.01738; 0.02934)

on where the neighbors are located. The average neighbor effect can be expected to be nearly zero, since the perturbation flow due to an isolated particle obtained by solving the EL equations (5), when averaged over a large volume around the particle, can be shown to be quite small. In comparison, the self-induced perturbation of each particle has a persistent component, and when averaged over many particles it appears to be about the same as that of an isolated particle. As a result, in Fig. 4 we observe "mean-SIV" and "mean" to be quite close.

A. Self-induced correction model

In this section, we evaluate the applicability of the self-induced velocity model, developed in [1,2] for an isolated particle, in the present finite volume fraction cases. We recall that they obtained their results by solving the governing equations (5) with $\phi_f(\mathbf{x}) = 1 - \phi_1(\mathbf{x})$ to represent only one particle at the center of the domain. The resulting nondimensional self-induced velocity correction is given as

$$u^{\mathrm{si}} = \frac{|\mathbf{F}|\,\psi_{\mathrm{os}}\,\chi\,\mathrm{Re}_\sigma}{3\pi\sqrt{2\pi}}, \tag{7}$$

where the analytic function obtained from Oseen's approximation is

$$\psi_{\mathrm{os}} = \frac{3}{\sqrt{2\pi}}\frac{\pi - \sqrt{2\pi}\mathrm{Re}_\sigma + (\pi/2)\mathrm{Re}_\sigma^2 - \pi e^{\mathrm{Re}_\sigma^2/2}\mathrm{erfc}(\mathrm{Re}_\sigma/\sqrt{2})}{\mathrm{Re}_\sigma^3}, \tag{8}$$

and the empirical nonlinear force correction obtained from numerical simulations is

$$\chi = 10^{A(\mathrm{Re}_\sigma)|\mathbf{F}|+B(\mathrm{Re}_\sigma)|\mathbf{F}|^2} \quad \text{with} \quad \begin{cases} A(\mathrm{Re}_\sigma) = 0.0213\exp\left(-3.16\mathrm{Re}_\sigma^{-0.88}\right), \\ B(\mathrm{Re}_\sigma) = 0.0027\exp\left(-5.54\mathrm{Re}_\sigma^{-0.76}\right). \end{cases} \tag{9}$$

In general, χ is typically close to unity.[1] It should be noted that for a constant $|\mathbf{F}|$, while $\psi_{\rm os}\chi$ decreases with Re_σ, $u^{\rm si}$ increases, as seen in Fig. 6.

We now apply this self-induced velocity estimation to a distribution of particles. To be precise, we evaluate the self-induced velocity of the lth particle located at $\mathbf{X}_l$. In an EL simulation that includes all the N particles, the input to the simulation around the point $\mathbf{X}_l$ is the local particle volume fraction $\phi_p(\mathbf{x}' + \mathbf{X}_l)$ and the feedback force $\mathbf{F}_{p\to f}(\mathbf{x}' + \mathbf{X}_l)$, where $\mathbf{x}' = \mathbf{x} - \mathbf{X}_l$ is centered about the lth particle. This results in the fluid velocity $\mathbf{u}_{@l}$ at the lth particle. Instead, in an EL simulation that includes only the $(N-1)$ particles, without the lth particle, the local particle volume fraction and the feedback force around $\mathbf{X}_l$ are given as

$$\phi_l^{\rm un}(\mathbf{x}') = \phi_p(\mathbf{x}' + \mathbf{X}_l) - \phi_1(\mathbf{x}') \quad \text{and} \quad \mathbf{F}_l^{\rm un}(\mathbf{x}') = \mathbf{F}_{p\to f}(\mathbf{x}' + \mathbf{X}_l) + \mathbf{e}_x\, G(\mathbf{x}'), \tag{10}$$

where the contribution from the lth particle has been subtracted. We denote the corresponding fluid velocity at $\mathbf{X}_l$ that would be computed in the $(N-1)$-particle EL simulation as $\mathbf{u}_{@l}^{\rm un}$. This is the undisturbed fluid velocity at the lth particle that we want to recover from $\mathbf{u}_{@l}$ that is available from the N-particle EL simulation.

In the case of an isolated particle, the self-induced velocity (7) was obtained by solving the linearized Oseen form of the governing equations (5) with undisturbed volume fraction and feedback force at the particle to be zero (i.e., there were no other particles). Now, in the presence of $(N-1)$ other particles, the undisturbed volume fraction and feedback force fields are nonzero and given in (10). The linearized Oseen form of the governing equations can again be solved to obtain the perturbation flow due to the introduction of the lth particle. From this we can obtain the self-induced velocity of the lth particle in the presence of $(N-1)$ other particles, which can be calculated as

$$u_{@l}^{{\rm si},M} = \left(\frac{1-\phi_{1c@l}}{1-\phi_{p@l}}\right)\frac{|\mathbf{F}_l|\,\psi_{\rm os}\,\chi\,\mathrm{Re}_{@l}^{\rm un}}{3\pi\sqrt{2\pi}}, \tag{11}$$

where the superscript "si, M" represents self-induced velocity predicted by the model. Three differences between the above and (7) for an isolated particle must be observed: (i) In the multiplicative factor contained within the parentheses, $\phi_{1c@l} = \phi_1(\mathbf{x}' = \mathbf{0})$ is the fluid volume fraction at $\mathbf{X}_l$ due to the presence of only the lth particle, and $\phi_{p@l} = \phi_p(\mathbf{x}' = \mathbf{0})$ is the fluid volume fraction at $\mathbf{X}_l$ in the presence of all the N particles. As we discussed earlier, for $\sigma/d_p = 2$, $\phi_{1c@l} \approx 1$, and as can be seen in Fig. 3, the fluid volume fraction at the particles varies around the average value of $1 - \langle\phi_p\rangle$. Thus, in general, the multiplicative factor increases above unity as the particle volume fraction increases. (ii) Since the undisturbed fluid velocity at the particles is different from the unit nondimensional ambient flow, the Reynolds number is calculated as $\mathrm{Re}_{@l}^{\rm un} = |\mathbf{u}_{@l}^{\rm un}|\sigma/\nu$. (iii) The function $\psi_{\rm os}$ must be computed based on $\mathrm{Re}_{@l}^{\rm un}$.

The feedback force and the self-induced correction of the lth particle must be solved simultaneously in a general implementation of the EL simulation. As pointed out earlier, the computed influence of neighbors in an EL simulation is not accurate to compute the correct force. We avoid this complication, by simplifying the problem with a constant unit nondimensional feedback force. However, as a result of the fixed feedback force, in general it will not be aligned along the undisturbed velocity $\mathbf{u}_{@l}^{\rm un}$ (or the EL velocity $\mathbf{u}_{@l}$). A vectorial version of the self-induced velocity estimation has been presented in [1], which must be used since the feedback force and undisturbed flow directions are not aligned. In the present EL simulations, we observe the effect of misalignment to be generally small. Furthermore, Eq. (11) is implicit due to the dependence of the Reynolds number on self-induced velocity. An approximation can be made to avoid the burden of an iterative solution of the implicit equation by estimating the Reynolds number $\mathrm{Re}_{@l}^{\rm un}$ based on the previous time step or with the uncorrected value, etc.

[1] We draw attention to a minor error in [2]. The force, which has been nondimensionalized by σ, must have been scaled by a factor $8\ln(2)$, which has been corrected above.

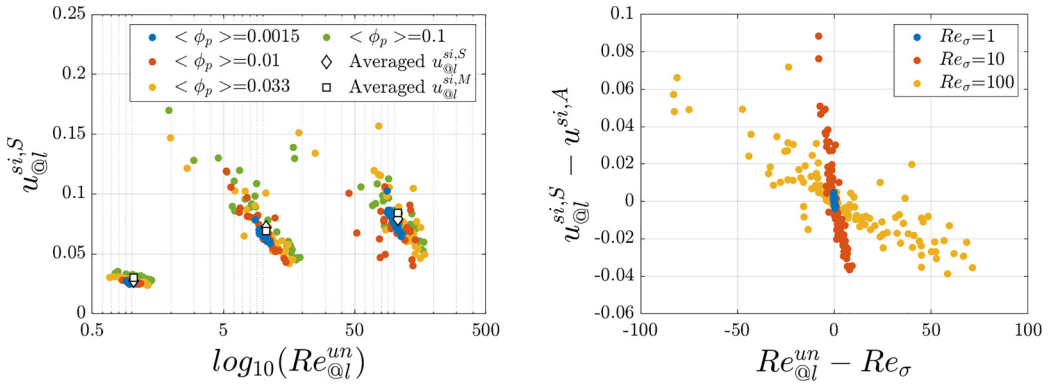

FIG. 7. (a) Self-induced velocity as a function of $\mathrm{Re}^{\mathrm{un}}_{@l}$. (b) A plot of $u^{\mathrm{si},S}_{@l} - u^{\mathrm{si},A}$ vs $\mathrm{Re}^{\mathrm{un}}_{@l} - \mathrm{Re}_\sigma$.

B. Model evaluation

We denote the x-component of self-induced velocity of the lth particle obtained from the EL simulation to be $u^{\mathrm{si},S}_{@l}$ and the corresponding quantity evaluated with the vector form of the model to be $u^{\mathrm{si},M}_{@l}$. Figure 7 presents a plot of $u^{\mathrm{si},S}_{@l}$ versus $\mathrm{Re}^{\mathrm{un}}_{@l}$ obtained from all the $(N-1)$-particle simulations. The different volume fraction cases are plotted in different colors, and the results of the three different Re_σ appear grouped as three clusters. For each Re_σ, the average self-induced velocity, averaged over the 120 EL simulations ($M = 30$ and 4 values of $\langle\phi_p\rangle$), is shown as open white diamond symbols. The corresponding average self-induced velocity obtained from the theoretical model is shown as open white squares. It is quite clear from their overlap that the model is able to capture the computed average self-induced velocity. Table II shows the mean and standard deviation of $u^{\mathrm{si},S}_{@l}$ and $u^{\mathrm{si},M}_{@l}$ for the 12 cases of different (Re_σ, $\langle\phi_p\rangle$) combinations. At the lower two Reynolds numbers, the simulation average shows a slight increase with increasing volume fraction. This increase is consistent with the volume fraction dependent multiplication factor that appears in the model [see (11)]. However, this increase is not clearly identified in the model average, partly due to the smaller sample size of $M = 30$.

In Fig. 7, from the scatter it can be gathered that the particle-to-particle variation in self-induced velocity is significant. The level of variation increases with both Re_σ and $\langle\phi_p\rangle$, and the corresponding standard deviations are presented in Table II. The table shows that while the model is reasonably accurate in predicting the average self-induced velocity, it is quite inaccurate in capturing the standard deviation. Specifically, the model overpredicts the standard deviation at the lowest Reynolds number, and incurs substantial underproduction as the Reynolds number increases.

The observed particle-to-particle variation in self-induced velocity is clearly due to the specific arrangement of neighbors. As a result of the manner in which the neighbors influence the local flow condition, $u^{\mathrm{si},S}_{@l}$ of some particles are higher than the average, while those of others are lower. Such particle-to-particle variation is also seen in the context of quasistudy drag force on a random distribution of particles subjected to a uniform flow [30–33]. The neighbor's influence can be considered to occur at two different levels. First, in the absence of the lth particle, the effect of neighbors is to change the undisturbed flow at $\mathbf{X}_l$ from the unit ambient flow. This effect of neighbors is accounted for in the particle-to-particle variation of its undisturbed ambient flow $\mathbf{u}^{\mathrm{un}}_{@l}$ (whose variation will be similar to that shown in Fig. 4). This in turn results in particle-to-particle variation in particle Reynolds number, $\mathrm{Re}^{\mathrm{un}}_{@l}$, which is plotted along the horizontal axis of Fig. 7. Second, in the presence of the lth particle, the local perturbation flow generated in response to its Gaussian feedback force does not appear to follow the behavior of an isolated particle subjected to a local uniform flow of $\mathbf{u}^{\mathrm{un}}_{@l}$, but it seems to be further influenced by the presence of the neighbors (also see [25]).

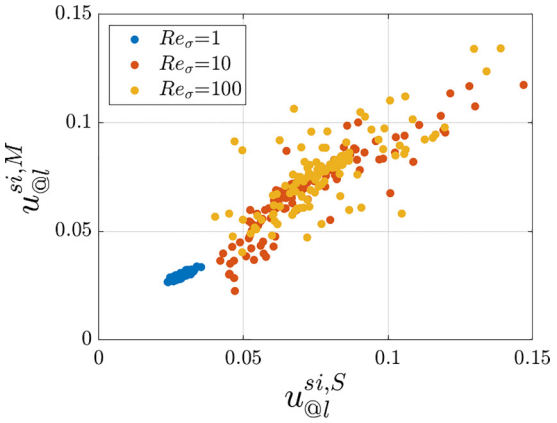

FIG. 8. A plot of predicted self-induced velocity using (12) vs actual values obtained from the EL simulations.

The most striking aspect of Fig. 7 is the negative correlation between $u^{\mathrm{si},S}_{@l}$ and $\mathrm{Re}^{\mathrm{un}}_{@l}$. With increasing undisturbed flow velocity, and the corresponding increase in $\mathrm{Re}^{\mathrm{un}}_{@l}$, the model (11) predicts the self-induced velocity to increase (this is the first effect discussed in the previous paragraph). The observed negative correlation clearly indicates the dominance of the second mechanism in generating the negative correlation. In other words, the arrangement of neighbors results in the undisturbed velocity of a particle being larger or smaller than the average, but this same arrangement of neighbors also alters the self-induced perturbation of the particle in such a way that the self-induced perturbation is larger (or smaller) when the undisturbed velocity is smaller (or larger). The reason for this negative correlation requires further investigation.

In Fig. 7(b) we plot fluctuating self-induced velocity $u^{\mathrm{si},S}_{@l} - u^{\mathrm{si},A}$ versus $\mathrm{Re}^{\mathrm{un}}_{@l} - \mathrm{Re}_\sigma$, where $u^{\mathrm{si},A}$ is the model prediction for a unit forcing at the average conditions of Re_σ and $\langle\phi_p\rangle$. The results for the three different Re_σ are presented in different colors, and negative linear regression coefficients β are obtained from these plots. We obtain $\beta = -0.0087$, -0.0058, and $-0.000\,57$ for $\mathrm{Re}_\sigma = 1$, 10, and 100, respectively. A simple empirical relation of the following form can predict the self-induced velocity of individual particles located within a random distribution:

$$u^{\mathrm{si},M}_{@l} = \left(\frac{1-\phi_{1c@l}}{1-\phi_{p@l}}\right)\frac{|\mathbf{F}_l|\,\psi_{\mathrm{os}}\,\mathrm{Re}_\sigma}{3\pi\sqrt{2\pi}} + \beta\left(\mathrm{Re}^{\mathrm{un}}_{@l} - \mathrm{Re}_\sigma\right), \tag{12}$$

where ψ_{os} is calculated based on the average Reynolds number Re_σ. The performance is evaluated by plotting this prediction against the simulation results in Fig. 8. The model is able to capture the observed, self-induced velocity quite well. It must, however, be cautioned that the regression coefficient β will not be a function of Re_σ, but it can be expected to depend on the Gaussian filter width and average volume fraction. Since the particle-to-particle variation in self-induced velocity is far weaker than the particle-to-particle variation in the influence of neighbors, here we will be satisfied with an accurate prediction of the average self-induced velocity, and we will not pursue modeling of particle-to-particle variation.

IV. DISCUSSION

In this section, we will discuss how the present findings apply to multiphase flow simulations by focusing on three aspects. First we will consider the limit of only two particles interacting in an EL simulation and use this to interpret the results for a random distribution of particles. Second, since the results of the previous section are for $\sigma/d_p = 2$, we will discuss how these results apply to other values of σ/d_p. Third, we will consider a practical implementation where the force on the particle,

and as a result the feedback force, will in turn be related to the undisturbed flow of the particle. Each will be considered below.

A. Two-particle interaction in an EL simulation

To understand the above-obtained results for a distribution of particles, here we will consider the much simpler problem of two-particle interaction. In an EL simulation, each particle will be fed back to the fluid in terms of the volume fraction and the feedback force, both of which are smoothed with a Gaussian. We consider two distinct limits: (i) the two particles being far apart, and (ii) the two particles overlapping each other. In the limit where the two particles are far apart, the self-induced velocity of each particle is unaffected by the presence of the other particle. As the particles approach each other, their mutual interaction becomes significant, and the self-induced velocity of a particle will deviate from the theoretical prediction (7) of an isolated particle. We want to quantify this influence of one on the self-induced velocity of the other.

The limiting case of two-particle interaction is when their feedback forces overlap on top of each other. Clearly, this is not possible in reality, since the two particles must be separated by the sum of their radii. This extreme case is considered here only as an example, since its analysis can be done easily. From (7), let the self-induced velocity of only one particle be $u_1^{\mathrm{si}} \propto |\mathbf{F}|\psi_{\mathrm{os}}\mathrm{Re}_\sigma\ \chi_1$, where $\mathbf{F}$ is the feedback force of a particle. Here the subscript "1" represents the result of a single particle. When two particles overlap, the feedback force doubles. For the same ambient flow, however, Re_σ remains the same, and also ψ_{os}, which only depends on Re_σ. The self-induced velocity of two overlapping particles is $u_2^{\mathrm{si}} \propto 2|\mathbf{F}|\psi_{\mathrm{os}}\mathrm{Re}_\sigma\ \chi_2$. Note that while χ_1 is evaluated using (9) as it is, χ_2 is evaluated with $\mathbf{F}$ replaced with $2\mathbf{F}$. The effect of one particle on the self-induced velocity of the other can be quantified by the ratio $(u_2^{\mathrm{si}}/2)/u_1^{\mathrm{si}}$, which can be approximated as

$$\frac{\left(u_2^{\mathrm{si}}/2\right)}{u_1^{\mathrm{si}}} = 10^{A(\mathrm{Re}_\sigma)|\mathbf{F}|+3B(\mathrm{Re}_\sigma)|\mathbf{F}|^2} \approx \chi_1, \tag{13}$$

where the approximation uses the fact that $B(\mathrm{Re}_\sigma)|\mathbf{F}|^2$ is usually much smaller than $A(\mathrm{Re}_\sigma)|\mathbf{F}|$. The interpretation is simple. In the self-induced velocity model given in (7), χ accounts for the nonlinear effect and therefore it is the nonlinear amplification factor when one particle overlaps another. It is important to note that while the self-induced velocity of a particle increases due to the presence of a neighbor, the local undisturbed flow of a particle, due to the presence of the other, decreases. This is consistent with the negative correlation seen in Fig. 7. In essence, in a distribution of particles, the increase in self-induced velocity accompanied by a reduction in local undisturbed flow is due to nonlinear interaction between the particles.

The self-induced velocity of two interacting particles is important in its own right, since in dilute systems a pair of particles do occasionally come close together to influence each other. However, the influence must now be considered properly as a function of the separation vector between the two particles relative to the ambient flow direction. By considering an array of two-particle EL simulations, one can construct a map of the nonlinear influence of a neighbor, much like the drag and lift perturbation maps that account for the influence of a neighbor on quasisteady force. As obtained above, χ offers a quick estimate of such a map when particles are very close to each other. Although overlapping particles are a limiting configuration, unfortunately, χ does not provide an upper bound, since at finite Re_σ the peak perturbation flow due to a Gaussian force is not at the center of the particle, but rather at several diameters downstream (see Fig. 2 of [2]). Nevertheless, $\chi - 1$ remains small over a wide range of Reynolds numbers and feedback force values, and therefore two-particle interaction in terms of self-induced velocity may in general be modest.

B. Effect of σ/d_p

The only parameter that was not varied in the Result section was σ/d_p. Its role can be established by looking at its effect on the volume fraction field. The Gaussian parameter σ is related to the

averaging volume, and given its value, the only quantity that determines how the volume fraction and feedback force vary over the triply periodic box is the number of particles contained within the averaging volume, which can be shown to be $\propto \langle\phi_p\rangle(\sigma/d_p)^3$. Thus, important quantities such as ratios of standard deviation to mean volume fraction and feedback force depend only on the parametric combination $\langle\phi_p\rangle(\sigma/d_p)^3$, which for the cases considered takes the values of 0.012, 0.08, 0.264, and 0.8. For example, the standard deviation to mean ratios of volume fraction measure in the simulations are $\sigma_\phi/\langle\phi_p\rangle = 0.895$, 0.335, 0.178, and 0.077, respectively. Thus, for any value of σ/d_p, other than that considered, the random distribution of particles will be the same as that considered in the present simulation, provided $\langle\phi_p\rangle(\sigma/d_p)^3$ is matched.

Only a limited range of values of σ/d_p is of interest to self-induced velocity estimation. For values of the ratio larger than 2.0, which was the value considered in the present simulations, the average self-induced correction will decrease in magnitude, which can be well predicted with (11). The particle-to-particle variation can also be inferred from the present results by matching $\langle\phi_p\rangle(\sigma/d_p)^3$. For $\sigma/d_p \gtrsim 6$, self-induced correction can be ignored altogether, since the particle becomes much smaller than the grid spacing. The value of σ/d_p cannot be too small either, since this will make the particle size much larger than the grid spacing. Also, from (3), $\sigma/d_p > 0.55$ for the volume fraction field to be larger than the close-packing limit at the center of the particle.

C. Implementation

We now briefly discuss a possible approach to implementing self-induced velocity correction in an EL simulation at a finite volume fraction. According to the present results, in order to predict the correct average self-induced correction in a distribution of particles, it is sufficient to use the same approach as that of an isolated particle, with the inclusion of a volume-fraction-dependent modification factor. More specifically, the model (11) can be used to calculate the self-induced velocity of a particle with the Reynolds number $\mathrm{Re}^{\mathrm{un}}_{@l}$ and volume fraction $\phi_{p@l}$ of that particle.

There is an important point to consider in an actual implementation. While our study here assumed a unit force, in an actual application $\mathbf{F}_l$ of each particle must be calculated based on the local relative velocity between the undisturbed fluid velocity and the particle velocity. But to calculate the undisturbed fluid velocity at the particle from the EL simulation, self-induced correction is needed, which in turn depends on the feedback force $\mathbf{F}_l$. This requires an implicit solution. We emphasize again that an accurate prediction of individual particle force is not possible even with self-induced velocity correction due to inaccuracy in the estimation of perturbation effects of neighbors in an EL simulation.

Finally, it must be stressed that the self-induced velocity predicted with the above implementation is accurate only in the average sense. The prediction will not accurately capture the particle-to-particle variation in the self-induced flow. Empirical relations such as those given in (12) can be used to better predict the self-induced velocities of individual particles. But such an approach may not be necessary, since the particle-to-particle variation in $\mathbf{u}_{@l}$ often will overwhelm the corresponding variation in self-induced flow.

V. CONCLUSIONS

It is now well accepted that a particle of size comparable to the local grid spacing results in substantial self-induced perturbation in a two-way coupled Euler-Lagrange (EL) simulation. This self-induced velocity must be subtracted from the computed EL fluid velocity to obtain the undisturbed velocity of the particle. Over the past decade, several analytical and numerical approaches have been advanced to estimate the self-induced velocity, which can be used to calculate the undisturbed ambient fluid velocity and the correct hydrodynamic force on the particle. These past efforts have all been in the limit of an isolated particle. The present work is an extension of these past efforts to address the question of self-induced velocity of a particle when it is surrounded

by neighbors. In other words, we consider the effect of a nonzero volume fraction in predicting the self-induced velocity of particles in an EL simulation.

Toward this end, in addition to performing EL simulations of flow over a random distribution of N stationary particles, we also perform 30 companion EL simulations of flow over $N-1$ particles, where in each companion simulation one particle has been removed from the original random distribution. Thus, each companion simulation allows a precise evaluation of both the undisturbed flow as well as the self-induced perturbation of the removed particle. Several hundred companion simulations have been performed to cover a range of Reynolds numbers and volume fractions. By analyzing the self-induced velocity obtained from these simulations, a number of key conclusions can be drawn, which are summarized as follows:

(i) A simple rederivation of Oseen's solution in the presence of volumetric and feedback force influence of neighbors shows that the self-induced velocity of an isolated particle obtained in earlier works [1,2] can still be used at a finite volume fraction with a modification factor $(1-\phi_{1c@l})/(1-\phi_{p@l})$, where $\phi_{p@l}$ is the particle volume fraction evaluated at the lth particle in the presence of all the particles, and $\phi_{1c@l}$ is the particle volume fraction at the lth particle in the presence of only that particle.

(ii) Simulation results show that the above simple volume fraction correction is quite accurate in predicting the average effect of volume fraction. That is, in a random distribution of particles of average volume fraction $\langle\phi_p\rangle$, the self-induced velocity averaged over all the particles can be well predicted with the above simple volume fraction modification. According to this model, the average self-induced velocity increases with increasing $\langle\phi_p\rangle$. The volume fraction effect has only been tested in the context of the Oseen solution model advanced in [1,2]. However, we expect the volume fraction modification to apply well for other proposed models as well in the prediction of the average self-induced velocity.

(iii) In a random distribution of particles, the velocity computed at a particle in an EL simulation deviates from the macroscale average due to both the particle's own self-induced perturbation and the perturbation flow induced by all other neighbors. With increasing volume fraction, the perturbation induced by neighbors far outweighs the self-induced velocity. However, when averaged over all the particles in a neighborhood, the perturbation influence of neighbors averages to zero, since this neighbor effect can be both positive and negative, whereas the self-induced perturbation is sustained and its average can make a substantial contribution.

(iv) In a random distribution of particles, the self-induced velocity of individual particles deviates from the average, and the standard deviation of particle-to-particle variation of self-induced velocity increases with increasing volume fraction. Predicting this variation is less important since it is typically much smaller than the particle-to-particle variation of neighbor-induced velocity. Nevertheless, it is observed that the self-induced velocity of a particle in a random distribution is higher or lower than the average depending on whether the particle's Reynolds number is lower or higher than the average. This negative correlation is surprising, since it is counter to the Reynolds number dependence of the self-induced velocity of an isolated particle. This illustrates the importance of nonlinear interactions. A simple one-parameter empirical modification can be developed to more accurately predict the self-induced velocity of individual particles in a random distribution.

ACKNOWLEDGMENTS

This work was sponsored by the Office of Naval Research (ONR) as part of the Multidisciplinary University Research Initiatives (MURI) Program, under Grant No. N00014-16-1-2617. The authors thank Saurabh Apte, Fabien Evrard, Berend van Wachem, and Jesse Capecelatro for illuminating discussions on this topic. This work was also partially supported and benefited from the U.S. Department of Energy, National Nuclear Security Administration, Advanced Simulation and Computing Program, as a Cooperative Agreement to the University of Florida under the Predictive Science Academic Alliance Program, under Contract No. DE-NA0002378.

[1] S. Balachandar and K. Liu, A correction procedure for self-induced velocity of a finite-sized particle in two-way coupled euler–lagrange simulations, Int. J. Multiphase Flow **159**, 104316 (2023).
[2] S. Balachandar, K. Liu, and M. Lakhote, Self-induced velocity correction for improved drag estimation in euler–lagrange point-particle simulations, J. Comput. Phys. **376**, 160 (2019).
[3] F. Battista, P. Gualtieri, J.-P. Mollicone, and C. M. Casciola, Application of the exact regularized point particle method (erpp) to particle laden turbulent shear flows in the two-way coupling regime, Int. J. Multiphase Flow **101**, 113 (2018).
[4] F. Battista, J.-P. Mollicone, P. Gualtieri, R. Messina, and C. M. Casciola, Exact regularized point particle (erpp) method for particle-laden wall-bounded flows in the two-way coupling regime, J. Fluid Mech. **878**, 420 (2019).
[5] E. Climent and M. R. Maxey, The force coupling method: A flexible approach for the simulation of particulate flows, in *Theoretical Methods for Micro Scale Viscous Flows* (Transworld Research Network, Kerala, India, 2009), pp. 1–21.
[6] M. Esmaily and J. A. K. Horwitz, A correction scheme for two-way coupled point-particle simulations on anisotropic grids, J. Comput. Phys. **375**, 960 (2018).
[7] F. Evrard, F. Denner, and B. van Wachem, Euler-lagrange modelling of dilute particle-laden flows with arbitrary particle-size to mesh-spacing ratio, J. Computat. Phys.: X **8**, 100078 (2020).
[8] T. Fukada, W. Fornari, L. Brandt, S. Takeuchi, and T. Kajishima, A numerical approach for particle-vortex interactions based on volume-averaged equations, Int. J. Multiphase Flow **104**, 188 (2018).
[9] T. Fukada, S. Takeuchi, and T. Kajishima, Interaction force and residual stress models for volume-averaged momentum equation for flow laden with particles of comparable diameter to computational grid width, Int. J. Multiphase Flow **85**, 298 (2016).
[10] P. Gualtieri, F. Picano, G. Sardina, and C. M. Casciola, Exact regularized point particle method for multiphase flows in the two-way coupling regime, J. Fluid Mech. **773**, 520 (2015).
[11] J. A. K. Horwitz, Improved force models for euler–lagrange computations, in *Modeling Approaches and Computational Methods for Particle-Laden Turbulent Flows* (Elsevier, Amsterdam, 2023), pp. 265–298.
[12] J. A. K. Horwitz, G. Iaccarino, J. K. Eaton, and A. Mani, The discrete green's function paradigm for two-way coupled euler–lagrange simulation, J. Fluid Mech. **931**, A3 (2022).
[13] J. A. K. Horwitz and A. Mani, Accurate calculation of stokes drag for point–particle tracking in two-way coupled flows, J. Comput. Phys. **318**, 85 (2016).
[14] J. A. K. Horwitz and A. Mani, Correction scheme for point-particle models applied to a nonlinear drag law in simulations of particle-fluid interaction, Int. J. Multiphase Flow **101**, 74 (2018).
[15] P. J. Ireland and O. Desjardins, Improving particle drag predictions in euler–lagrange simulations with two-way coupling, J. Comput. Phys. **338**, 405 (2017).
[16] N. A. Keane, S. V. Apte, S. S. Jain, and M. A. Khanwale, Effect of interpolation kernels and grid refinement on two way-coupled point-particle simulations, Int. J. Multiphase Flow **166**, 104517 (2023).
[17] T. Lesaffre, A. Pestre, E. Riber, and B. Cuenot, Correction methods for exchange source terms in unstructured Euler-Lagrange solvers with point-source approximation, Flow Turbul. Combust. **112**, 831 (2023).
[18] K. Liu, M. Lakhote, and S. Balachandar, Self-induced temperature correction for inter-phase heat transfer in euler-lagrange point-particle simulation, J. Comput. Phys. **396**, 596 (2019).
[19] S. Lomholt and M. R. Maxey, Force-coupling method for particulate two-phase flow: Stokes flow, J. Comput. Phys. **184**, 381 (2003).
[20] M. R. Maxey and B. K. Patel, Localized force representations for particles sedimenting in stokes flow, Int. J. Multiphase Flow **27**, 1603 (2001).
[21] P. Pakseresht and S. V. Apte, A disturbance corrected point-particle approach for two-way coupled particle-laden flows on arbitrary shaped grids, J. Comput. Phys. **439**, 110381 (2021).
[22] P. Pakseresht, M. Esmaily, and S. V. Apte, A correction scheme for wall-bounded two-way coupled point-particle simulations, J. Comput. Phys. **420**, 109711 (2020).
[23] Y. Pan and S. Banerjee, Numerical simulation of particle interactions with wall turbulence, Phys. Fluids **8**, 2733 (1996).

[24] J.-F. Poustis, J.-M. Senoner, D. Zuzio, and P. Villedieu, Regularization of the lagrangian point force approximation for deterministic discrete particle simulations, Int. J. Multiphase Flow **117**, 138 (2019).
[25] S. Apte, A zonal advection-diffusion-reaction model for self-disturbance correction in point-particle computations, in *Center for Turbulence Research-Proceedings of the Summer Program* (Standford University, 2022).
[26] J. Capecelatro and O. Desjardins, An euler–lagrange strategy for simulating particle-laden flows, J. Comput. Phys. **238**, 1 (2013).
[27] K. Liu, M. Allahyari, J. S. Salinas, N. Zgheib, and S. Balachandar, Peering inside a cough or sneeze to explain enhanced airborne transmission under dry weather, Sci. Rep. **11**, 9826 (2021).
[28] K. Liu, P. D. Huck, A. Aliseda, and S. Balachandar, Investigation of turbulent inflow specification in euler–lagrange simulations of mid-field spray, Phys. Fluids **33**, 033313 (2021).
[29] B. Siddani, S. Balachandar, J. Zhou, and S. Subramaniam, Investigating the influence of particle distribution on force and torque statistics using hierarchical machine learning, AIChE J. e18339 (2024).
[30] G. Akiki, T. L. Jackson, and S. Balachandar, Force variation within arrays of monodisperse spherical particles, Phys. Rev. Fluids **1**, 044202 (2016).
[31] G. Akiki, T. L. Jackson, and S. Balachandar, Pairwise interaction extended point-particle model for a random array of monodisperse spheres, J. Fluid Mech. **813**, 882 (2017).
[32] Z. Cheng and A. Wachs, Hydrodynamic force and torque fluctuations in a random array of polydisperse stationary spheres, Int. J. Multiphase Flow **167**, 104524 (2023).
[33] A. Seyed-Ahmadi and A. Wachs, Microstructure-informed probability-driven point-particle model for hydrodynamic forces and torques in particle-laden flows, J. Fluid Mech. **900**, A21 (2020).